Transworld Research Network
37/661 (2), Fort P.O., Trivandrum-695 023, Kerala, India

Recent Res. Devel. Acoustics, 1(2003): 39-67 ISBN: 81-7895-083-9

3 Acoustic radiation forces: Classical theory and recent advances

Alexander A. Doinikov
Institute of Nuclear Problems, Belarus State University, 11 Bobruiskaya Street
Minsk 220050, Belarus

Abstract

The review presents an account of the historical development and the current state of the theory of acoustic radiation forces. These forces are induced by a sound wave field on dispersed particles (gas bubbles, liquid drops, particles of dust, etc.) suspended in a fluid and make them drift, cluster in certain space areas, interact with each other, etc. The early theory of this phenomenon is based on a large number of simplifying assumptions, which restrict its capabilities and do not allow one to explain many experimental observations. Recent extensive studies have fundamentally generalized the original theory of acoustic radiation forces and made it possible to understand experimental findings that appeared abnormal within the framework of the early theory, as well as to predict new interesting effects.

Correspondence/Reprint request: Dr. Alexander A. Doinikov, Institute of Nuclear Problems, Belarus State University, 11 Bobruiskaya Street, Minsk 220050, Belarus. E-mail: doinikov@inp.minsk.by

Introduction

When a fluid (liquid or gas) with foreign inclusions (gas bubbles, liquid drops, solid particles, etc.) is irradiated by a sound field, the suspended particles experience steady (time-averaged) hydrodynamic forces which make them drift, cluster at certain space points, attract or repel one another, etc. These forces are called *acoustic radiation forces*, or *acoustic radiation pressure*. They are an analog of the optical radiation pressure exerted by an electromagnetic wave on electrically or magnetically responsive objects [1,2]. But the acoustic radiation forces are in general much larger than their electromagnetic counterpart. Therefore they are found useful in a variety of scientific and technical applications, such as acoustic levitation [3,4], calibration of sound transducers [5], acoustic coagulation of aerosols [6,7], biomedical ultrasonics [8], etc., and also play an important role in many other acoustic phenomena, such as acoustic cavitation and sonoluminescence [9-12].

It is conventional to divide the acoustic radiation forces into two types, namely, *primary forces*, which are experienced by single particles, and *secondary forces*, which are responsible for particle-particle interactions. The primary forces cause particles to migrate in an acoustic field or to gather in certain areas, such as pressure antinodes (or nodes) of standing sound waves, while the secondary forces make them attract or repel one another, and sometimes form stable multi-particle structures. The forces on gas bubbles are normally referred to as *Bjerknes forces* after C.A. Bjerknes and his son V.F.K. Bjerknes, who were the first to report on such forces [13]. The interaction forces between solid particles are sometimes called *König forces* in honor of W. König, who first derived an analytical expression for the interaction force between two rigid spheres in a fluid flow and used it to account for particle coagulation in a sound field. [14].

Since the nineteenth century, the effect of acoustic radiation forces was the subject of much theoretical work. The early (classical) theory of this phenomenon was based on a large number of simplifying assumptions, which restricted essentially its accuracy and area of applicability and did not allow this theory to account for many posterior experimental observations, such as stable bubble clusters known as *bubble grapes* [15,16], bunching solid particles in a high-viscosity liquid subject to a standing ultrasonic wave around the velocity nodes instead of antinodes [17], acoustic streamer formation [9,18], etc. Recent extensive studies have fundamentally generalized the original theory of acoustic radiation forces. As a result, it became possible to understand a number of experimental findings that appeared abnormal within the framework of the classical theory, as well as to predict new interesting effects. It is the purpose of this review to give an account of the historical development and the current state of the theory of acoustic radiation forces. The review does not pretend to present an exhaustive coverage of all relevant works since the literature on the subject is greatly extensive. Emphasis will be placed on the most important theoretical results and recent developments.

1. Primary forces

The first thorough theoretical research on the primary acoustic radiation forces is due to King [19]. He obtained a general formula for the radiation force that is exerted by an axisymmetric sound field on a rigid sphere of arbitrary radius freely suspended in an

ideal fluid. In practice, however, one deals mainly with particles of a size much smaller than the wavelength of sound in the host fluid. Therefore King also derived the corresponding limiting expressions for the radiation forces in a plane traveling wave and a plane standing wave. They are given, respectively, by

$$F_{rs}^{(tr)} = 2\pi\rho_0|A|^2(kR_0)^6\frac{9+2(1-\lambda_\rho)^2}{9(2+\lambda_\rho)^2}, \tag{1.1a}$$

$$F_{rs}^{(st)} = \pi\rho_0|A|^2\sin(2kd)(kR_0)^3\frac{5-2\lambda_\rho}{3(2+\lambda_\rho)}, \tag{1.1b}$$

where ρ_0 is the fluid density at rest, A the complex amplitude of the velocity potential of the imposed sound field, $k=\omega/c$ the wavenumber in the fluid, ω the angular driving frequency, c the speed of sound in the fluid, R_0 the radius of the sphere (note that, by assumption, $kR_0 \ll 1$), $\lambda_\rho = \rho_0/\tilde{\rho}$, $\tilde{\rho}$ the density of the sphere, d the distance between the equilibrium center of the sphere and the nearest velocity node plane of the standing sound wave, and the subscript "rs" means "rigid sphere".

King's theory gave an insight into why dispersed particles, such as aerosol droplets and airborne dust, accumulate in a standing sound wave field near either the velocity nodes or the velocity antinodes. Equation (1.1b) shows that the above regions are positions of stable equilibrium for solid particles, so that "heavy" particles, with $\tilde{\rho} > 0.4\rho_0$, accumulate at the velocity antinodes, while "light" particles, with $\tilde{\rho} < 0.4\rho_0$, at the velocity nodes. Experiments on spheres, compressibility of which is small compared with that of the surrounding fluid (this condition is just approximated by the model of rigid sphere), demonstrate that Eq. (1.1b) is also in good quantitative agreement with experimental data [20-22]. Note, however, that all these experiments were carried out under conditions where dissipative effects were negligible. As for a quantitative check of Eq. (1.1a), i.e., making a comparison between measured values of the radiation force in a traveling wave and values calculated from Eq. (1.1a), the author is not aware of such experiments. Judging from the available literature, they have just not been conducted. We will turn back to this point below to show that ignoring viscous effects in Eq. (1.1a) leads to vastly underestimating the magnitude of the radiation force. Next, Eq. (1.1a) shows that solid particles are always urged by a traveling wave away from the sound source, which appears reasonable, but we will see below that dissipative effects can correct this conclusion as well.

Although his approach can be applied to any axisymmetric acoustic field, King restricted himself to the two types of waves considered above. The radiation force on a rigid sphere in a spherical sound field was calculated and studied by Embleton [23,24], Nyborg [25], and Hasegawa *et al*. [26]. Embleton also examined the case of a cylindrical wave filed [27]. We will not dwell on these cases. It should only be emphasized that all of these authors assumed the host fluid to be ideal.

Despite the achievements of King's theory, it was clear that the model of rigid sphere would hardly be adequate if the compressibility of a body is comparable to or much larger than that of the host fluid, as with a gas bubble in a liquid or a liquid drop placed in a different, immiscible liquid. Realizing this problem, Yosioka and Kawasima [28] applied the equations of motion of an ideal compressible fluid to both the host fluid

and the medium inside the particle involved, allowing thereby that the particle is of finite compressibility and keeps the spherical shape only at rest. Like King, they first derived a general formula for the radiation force, which is valid for a sphere of arbitrary size and compressibility, and then obtained approximate expressions for the forces on a liquid drop and a gas bubble in a plane traveling wave and a plane standing wave in the limit of long sound wavelength, i.e., for $kR_0 \ll 1$. These expressions are as follows:

$$F_d^{(tr)} = \frac{2\pi\rho_0|A|^2(kR_0)^6}{9(2+\lambda_\rho)^2}\left\{\left[3-(2+\lambda_\rho)\lambda_\rho\frac{c^2}{\tilde{c}^2}\right]^2+2(1-\lambda_\rho)^2\right\}, \tag{1.2a}$$

$$F_d^{(st)} = \frac{\pi}{3}\rho_0|A|^2\sin(2kd)(kR_0)^3\left(\frac{5-2\lambda_\rho}{2+\lambda_\rho}-\frac{\lambda_\rho c^2}{\tilde{c}^2}\right), \tag{1.2b}$$

$$F_b^{(tr)} = \frac{2\pi\rho_0|A|^2(kR_0)^2}{(1-\omega_0^2/\omega^2)^2+\delta_{rad}^2}, \tag{1.3a}$$

$$F_b^{(st)} = \frac{\pi\rho_0|A|^2kR_0(1-\omega_0^2/\omega^2)\sin(2kd)}{(1-\omega_0^2/\omega^2)^2+\delta_{rad}^2}, \tag{1.3b}$$

where R_0 is now the equilibrium radius of the particle involved (a drop or a bubble), $\tilde{\rho}$ the equilibrium density of the particle, $\tilde{c}$ the speed of sound inside the particle, $\delta_{rad} = kR_0$ the radiation damping constant, and ω_0 the fundamental resonance frequency of the bubble, given by [29] $\omega_0 = (\tilde{c}/R_0)\sqrt{3/\lambda_\rho} = \sqrt{3\tilde{\gamma}P_0/\rho_0 R_0^2}$, P_0 denoting the hydrostatic pressure in the host fluid.

In the limit $c/\tilde{c} \to 0$, Eqs. (1.2a) and (1.2b), which give the forces on drops, turn into King's formulas. In the general case, however, the behavior of a drop and a solid particle is not identical. In the case of a bubble, Eqs. (1.3a) and (1.3b), distinctions from King's formulas are even more essential. Equations (1.3a) and (1.3b), first, is of lower order in the small parameter kR_0, and second, contain the resonant factor in the denominator. As a result, the radiation forces on bubbles are in general much larger than the forces on solid particles and drops, all other things being equal. Equation (1.3b) also shows that in a standing wave field, "small" bubbles, with $\omega_0 > \omega$, should gather at the pressure antinodes, while "large" bubble, with $\omega_0 < \omega$, at the pressure nodes. All these predictions are in qualitative agreement with experiments [28,30-34]. Crum [35] and Eller [36] carried out measurements of the primary radiation forces on, respectively, drops and bubbles in standing waves. In both cases, a satisfactory quantitative agreement with Eqs. (1.2b) and (1.3b) was obtained. No quantitative check of Eq. (1.2a) was made. Whereas the analogous equation for bubbles, Eq. (1.3a), was tested by its authors, Yosioka and Kawasima [28], who found a considerable difference between calculated and experimental values of the force. [The surprising thing is that this fact did not cast any doubt on the analogous formulas for solid particles and drops, Eqs. (1.1a) and (1.2a).] To alleviate the disagreement, Yosioka and Kawasima allowed for heat loss that occurs in the process of volume oscillations of a bubble and obtained a refined result [33], which can be represented as

$$F_b^{(tr)} = \frac{2\pi\rho_0|A|^2 k R_0(\delta_{rad}+\delta_{th})}{(1-\omega_0^2/\omega^2)^2+(\delta_{rad}+\delta_{th})^2}, \tag{1.4}$$

with the thermal damping constant δ_{th} defined by

$$\delta_{th} = \frac{3(\tilde{\gamma}-1)\left[X(\sinh X+\sin X)-2(\cosh X-\cos X)\right]\omega_0^2}{X\left[X(\cosh X-\cos X)+3(\tilde{\gamma}-1)(\sinh X-\sin X)\right]\omega^2}. \tag{1.5}$$

Here, $X = R_0(2\omega/\tilde{\chi})^{1/2}$, $\tilde{\gamma}$ and $\tilde{\chi}$ are, respectively, the ratio of specific heats and the thermal diffusivity of the gas in the bubble, and the resonance frequency ω_0 is given by a refined formula

$$\omega_0 = \frac{1}{R_0}\left(\frac{3\tilde{\gamma}P_0}{\rho_0}\right)^{1/2}\left[1+\frac{3(\tilde{\gamma}-1)(\sinh X-\sin X)}{X(\cosh X-\cos X)}\right]^{-1/2}. \tag{1.6}$$

Equation (1.3b) was refined by Crum and Eller [37], who included the effects of heat conduction and viscosity on the bubble pulsations. Their resulting expression is identical in form to Eq. (1.3b),

$$F_b^{(st)} = \frac{\pi\rho_0|A|^2 k R_0(1-\omega_0^2/\omega^2)\sin(2kd)}{(1-\omega_0^2/\omega^2)^2+\delta^2}, \tag{1.7}$$

but δ_{rad} is replaced with the total damping constant $\delta = \delta_{rad}+\delta_{th}+\delta_{vis}$, where δ_{th} is calculated from Eq. (1.5) and the viscous damping constant is given by $\delta_{vis} = 4\nu/\omega R_0^2$, with ν denoting the kinematic viscosity of the host fluid. In addition, the resonance frequency of the bubble is defined as $\omega_0 = \sqrt{3\tilde{\gamma}_{ef}P_0/\rho_0 R_0^2}$, where

$$\tilde{\gamma}_{ef} = \tilde{\gamma}\left\{\left(1+\frac{\omega^4\delta_{th}^2}{\omega_0^4}\right)\left[1+\frac{3(\tilde{\gamma}-1)(\sinh X-\sin X)}{X(\cosh X-\cos X)}\right]\right\}^{-1}. \tag{1.8}$$

There is a series of articles by Hasegawa *et al.* [38-45] in which the acoustic radiation force on an elastic sphere is investigated. The common objective of these investigations is the improvement of the techniques of absolute acoustic intensity determination by the radiation force method. In the first article of the series, [38], an expression is derived for the force exerted by a plane traveling wave on an elastic sphere of arbitrary radius freely suspended in an ideal fluid. This expression is then used in numerical calculations of the forces on brass and steel spheres in water results of which are compared with predictions of King's theory. It is shown that in the long sound wavelength limit ($k R_0 \ll 1$), the effect of elasticity is negligible. Deviations from King's theory appear for $k R_0 \geq 2$ and give rise to sharp maximums or minimums in the radiation force versus $k R_0$ curves, which correspond to resonance in every normal mode of the free vibration of the sphere involved. Experiments made by the authors showed good agreement with their theory. The next papers, [39-42], present extensive numerical and experimental investigations of the radiation forces exerted by a plane traveling wave field on spheres of various materials. Note, however, that these experiments cannot be used for a quantitative check of Eqs. (1.1a) and (1.2a) since they are restricted to $k R_0 \geq 1$.

The papers [43-45] examine the behavior of elastic spheres in sound fields of different type, such as a plane standing wave and a plane quasistationary (part traveling and part standing) wave [43,44] and a diverging spherical wave [45].

Bearing in mind applications such as acoustic levitation in containerless processing and medical ultrasound equipment, Wu and Du [46] calculated the radiation force on a small compressible sphere placed on the axis of a focused sound beam. Their study shows that the physical focal point of a focused beam is a stable point for rigid spheres with $\tilde{\rho} > 0.4\rho_0$ and hence focused sound beams may be an alternative for levitating small high-density samples. It was also found that the focal point is a stable potential well for small bubbles, with $\omega_0 > \omega$, and they can be trapped there, like bubbles in the pressure antinodes of a standing wave. In relation to acoustic levitation, it is pertinent to mention one more work. As pointed out above, the effect of acoustic radiation pressure is used in containerless technology, in which materials are processed under acoustic levitation. This technology usually requires the heating and cooling of the samples. Therefore it is desirable to know how the acoustic radiation force on the sample is affected by the temperature difference between the sample and the environment. This effect is studied in [47].

The theory outlined up to here may be called classical. Because the basic assumption on which all the studies cited above are based remains intact since King's paper. This is the assumption that the host fluid is ideal, i.e., nonviscous and non-heat-conducting. Attempts made by some authors to take account of dissipative effects on the radiation force, as in [33,37], cannot be considered to be satisfactory from the standpoint of generality and rigor. Moreover, as we will see below, they are justified only for weak dissipation. A valid transition to a real fluid must include the following obligatory steps. (i) The fluid motion should be described by the Navier-Stokes equation instead of the Euler equation. (ii) The equations of fluid motion should be supplemented with the equation of heat transfer. (iii) Viscosity gives rise to a vortical component in the fluid motion, which should be taken into account. (iv) The boundary conditions at the particle surface get more complicated. In an ideal fluid, there are two boundary conditions: continuity of the normal components of the fluid velocity and stress across the particle surface. In a viscous heat-conducting fluid, there are in general six boundary conditions: continuity of the normal and tangential components of the velocity and stress and continuity of temperature and heat flux. (v) Calculation of radiation forces in a real fluid requires solving not only the linearized equations of fluid motion, but the so-called equations of acoustic streaming as well. These equations are obtained by time averaging the viscous equations of fluid motion and keeping up to second-order terms in the amplitude of the incident acoustic field [48]. Finding their solutions is the main problem of the calculation of the radiation forces in a real fluid. All of the above-listed operations, with minimal restrictions on the parameters of the task, were first performed by Doinikov [49-51]. His theory provides a general formula for the acoustic radiation force exerted by an axisymmetric sound field on a spherical (at rest) particle immersed in a viscous heat-conducting fluid. No restrictions are imposed on the particle size, which means that the particle can be of arbitrary radius with respect to the sound, viscous, and thermal wavelengths in the host fluid. The above wavelengths are supposed to be arbitrary relative to one another as well. The obtained formula for the radiation force is also general in that it can be applied to any of the following objects: a gas bubble, a

liquid drop, a rigid or elastic sphere, a spherical shell, etc. In the general case, the radiation force is expressed in terms of the linear scattering coefficients to be determined by the particle type. Thus, to obtain the force on a specific particle, the problem of linear scattering for that particle should only be solved. Such problems are normally not difficult mathematically unless the particle has a complicated internal structure. The application of the general theory to dispersed particles of most interest (rigid sphere, drop, bubble) was carried out in three following papers, [52-54].

Let us begin with [52], where the force on a rigid sphere is examined, and compare its results with King's theory. Since the general formula for the force is extremely intricate, it is analyzed in [52] for two limiting cases: $R_0 \gg \delta_v, \delta_t, \tilde{\delta}_t$ and $R_0 \ll \delta_v, \delta_t, \tilde{\delta}_t$, it being also assumed that in both cases $R_0, \delta_v, \delta_t, \tilde{\delta}_t \ll \lambda_s$. Here, $\delta_v = \sqrt{2\nu/\omega}$ and $\delta_t = \sqrt{2\chi/\omega}$ are the viscous and thermal penetration depths in the host fluid, χ is the thermal diffusivity of the fluid, $\tilde{\delta}_t = \sqrt{2\tilde{\chi}/\omega}$ is the thermal penetration depth in the sphere material, and λ_s is the sound wavelength in the fluid (notice that $\tilde{\lambda}_s, \tilde{\delta}_v \to \infty$ as the sphere is rigid). In the first case, which corresponds to *weak* dissipation, the forces in a plane traveling wave and a plane standing wave are found to be

$$F_{rs}^{(tr)} = 6\pi\rho_0 |A|^2 (kR_0)^3 \left[\left(\frac{1-\lambda_\rho}{2+\lambda_\rho} \right)^2 \frac{\delta_v}{R_0} + \frac{\gamma - 1}{6(1+\lambda_\kappa \tilde{\delta}_t/\delta_t)} \frac{\delta_t}{R_0} \right], \tag{1.9a}$$

$$F_{rs}^{(st)} = \pi\rho_0 |A|^2 \sin(2kd)(kR_0)^3 \left[\frac{5-2\lambda_\rho}{3(2+\lambda_\rho)} + O\left(\frac{\delta_v}{R_0}, \frac{\delta_t}{R_0} \right) \right], \tag{1.9b}$$

where γ is the ratio of specific heats in the fluid, $\lambda_\kappa = \kappa/\tilde{\kappa}$, and κ and $\tilde{\kappa}$ are the thermal conductivities of the fluid and the sphere material, respectively.

Comparison of Eqs. (1.1b) and (1.9b) shows that in a standing wave, weak dissipation only gives rise to a small correction to King's result, which explains good agreement between Eq. (1.1b) and experiments [20-22]. In a traveling wave, however, this is not the case. Equations (1.1a) and (1.9a) are totally different. We will understand why this occurs if we recall that both Eq. (1.1a) and Eq. (1.9a) are terms of a single expansion of the radiation force in the small parameters kR_0, δ_v/R_0, and δ_t/R_0. When the dissipative effects are zero, the leading term of the expansion is given by Eq. (1.1a). When they are small but nonzero, Eq. (1.9a) is dominant as it is of lower order in kR_0, which is the smallest parameter of the expansion. Conditions under which Eq. (1.9a) predominates are given by

$$(kR_0)^3 \ll \delta_v/R_0 \ll 1 \quad \text{or/and} \quad (kR_0)^3 \ll \delta_t/R_0 \ll 1. \tag{1.10}$$

Consideration of specific situations shows that in most cases of interest Eqs. (1.10) are well satisfied [55]. This means that the radiation force on a small rigid sphere in a plane traveling wave, in the limit of low dissipation, is determined by Eq. (1.9a) rather than King's formula (1.1a) and, accordingly, should be much greater in magnitude. The cause of why the failure of Eq. (1.1a) was not discovered previously is likely to be lack of due experimental measurements.

In the second limit ($R_0 \ll \delta_v, \delta_t, \tilde{\delta}_t$), which corresponds to *strong* dissipation, one has

$$F_{rs}^{(tr)}=\frac{2}{3}\pi\rho_0|A|^2(kR_0)^3\left[\frac{11(\lambda_\rho-1)}{5\lambda_\rho}\frac{R_0}{\delta_v}-\frac{(\gamma-1)\lambda_\chi}{\lambda_\kappa}\frac{R_0}{\delta_t}\right], \tag{1.11a}$$

$$F_{rs}^{(st)}=\pi\rho_0|A|^2\sin(2kd)(kR_0)^3\left[\frac{2\lambda_\rho-1}{3\lambda_\rho}+O\left(\frac{R_0}{\delta_v},\frac{R_0}{\delta_t}\right)\right], \tag{1.11b}$$

where $\lambda_\chi=\chi/\tilde{\chi}$. According to Eq. (1.11a), in the limit of strong dissipation, the force exerted by a traveling wave on spheres with $\tilde{\rho}>\rho_0$ is directed toward the sound transducer. Spheres with $\tilde{\rho}<\rho_0$ can move both away from the sound transducer and toward it depending on whether the first or the second of the two terms in square brackets in Eq. (1.11a) is dominant. Equation (1.11b) shows that in a standing wave, spheres with $\tilde{\rho}>2\rho_0$ are attracted to the velocity nodes, while spheres with $\tilde{\rho}<2\rho_0$, to the velocity antinodes. Comparing this result with Eq. (1.9b), one can see that under strong dissipation spheres with $\tilde{\rho}<0.4\rho_0$ or $\tilde{\rho}>2\rho_0$ behave inversely. Most of experiments where the behavior of solid particles in a plane standing wave field is investigated fall into the limit of low dissipation. For example, in [21] and [22] the magnitude of R_0/δ_v exceeds 9 and 98, respectively. Therefore it is no wonder that they demonstrate agreement with Eq. (1.9b). There is, however, one experiment [17] which can be attributed to the case of manifest dissipation. In this experiment, the motion of micron-sized steel particles in water, ethyl alcohol, and glycerin in the presence of a plane standing ultrasonic wave was observed. It was found that in some cases the particles did really accumulate at the velocity nodes, which counts in favor of Eq. (1.11b).

In [53], the case of a liquid drop is analyzed. The two limits similar to those considered above are defined as $\lambda_s,\tilde{\lambda}_s\gg R_0\gg\delta_v,\tilde{\delta}_v,\delta_t,\tilde{\delta}_t$ and $\lambda_s,\tilde{\lambda}_s\gg\delta_v,\tilde{\delta}_v,\delta_t,\tilde{\delta}_t\gg R_0$, where $\tilde{\lambda}_s$ and $\tilde{\delta}_v$ are the sound wavelength and the viscous penetration depth inside the drop. In the first of them, weak dissipation, for a plane traveling wave, one has

$$F_d^{(tr)}=2\pi\rho_0|A|^2(kR_0)^3\left[T_v\frac{\delta_v}{R_0}+T_t\frac{\delta_t}{R_0}\right], \tag{1.12}$$

where

$$T_v=\frac{3(1-\lambda_\rho)^2\left[1+\lambda_\rho\delta_v/\tilde{\delta}_v+2\lambda_\eta\tilde{\delta}_v/R_0+2(\lambda_\eta\tilde{\delta}_v/R_0)^2+2\lambda_\rho\lambda_\eta\delta_v/R_0\right]}{(2+\lambda_\rho)^2\left[(1+\lambda_\rho\delta_v/\tilde{\delta}_v+\lambda_\eta\tilde{\delta}_v/R_0)^2+(\lambda_\eta\tilde{\delta}_v/R_0)^2\right]}, \tag{1.13}$$

$$T_t=\frac{(1-\lambda_\kappa\tilde{\delta}_t^2/\lambda_\alpha\delta_t^2)\left[\gamma-1-(\tilde{\gamma}-1)\lambda_\alpha\lambda_\rho c^2/\tilde{c}^2\right]}{2(1+\lambda_\kappa\tilde{\delta}_t/\delta_t)}, \tag{1.14}$$

$\lambda_\eta=\eta/\tilde{\eta}$, $\lambda_\alpha=\alpha/\tilde{\alpha}$, η is the dynamic viscosity of the host fluid, α is the volume thermal expansion coefficient of the host fluid, and the tilde denotes similar quantities that concern the medium inside the drop. Comparing Eqs. (1.12) and (1.2a), it is easily seen that the difference between them is of the same character as between Eqs. (1.9a) and (1.1a). Thus, what was said of Eq. (1.9a) is also true for Eq. (1.12). In particular, that in most cases, as estimates show, Eq. (1.2a) is just a small correction to Eq. (1.12).

The expression for the force in a plane standing wave is omitted here because it is identical to Eq. (1.2b), except for small dissipation corrections.

In the limit of strong dissipation, the forces on a drop are given by

$$F_d^{(tr)} = \frac{1}{3}\pi\rho_0|A|^2(kR_0)^3\left(\frac{\delta_v}{R_0}\right)^2\left[\frac{\gamma-1}{\lambda_\alpha} - \frac{\tilde{\gamma}\lambda_\rho c^2}{\tilde{c}^2} - 2 - 4\,\mathrm{Re}(\Lambda)\right], \tag{1.15a}$$

$$F_d^{(st)} = \frac{2}{3}\pi\rho_0|A|^2\sin(2kd)(kR_0)^3\left(\frac{\delta_v}{R_0}\right)^2 \mathrm{Im}(\Lambda), \tag{1.15b}$$

where

$$\Lambda = \frac{3+16\lambda_\eta - 19/\lambda_\eta + 4\sigma(k_v R_0)^2(5+2\lambda_\eta)/\rho_0\omega^2 R_0^3}{89+48\lambda_\eta + 38/\lambda_\eta - 40\sigma(k_v R_0)^2(1+\lambda_\eta)/\rho_0\omega^2 R_0^3}, \tag{1.16}$$

σ is the surface tension, and $k_v = (1+i)/\delta_v$ is the viscous wavenumber in the host fluid.

It is of interest to compare Eq. (1.15a) with the similar formula for a rigid sphere, Eq. (1.11a). The comparison shows that under strong dissipation the difference between the force on a rigid sphere and the force on a drop is much larger than in the limit of weak dissipation. When dissipation is weak, the forces are approximately on the same order, while under strong dissipation the magnitude of the force acting on a drop is much larger, other things being equal. According to Eq. (1.16), $\mathrm{Im}(\Lambda) > 0$. It follows that in a plane standing wave all drops, regardless of their properties, are attracted to the velocity antinodes.

Finally, let us turn to [54], which deals with the radiation force on a gas bubble. In the limit of weak dissipation, [54] gives

$$F_b^{(tr)} = \frac{2\pi\rho_0|A|^2 kR_0}{(1-\omega_0^2/\omega^2)^2+\Delta^2}\left[\delta_{rad} + \frac{3(\tilde{\gamma}-1)\omega_0^2\tilde{\delta}_t}{2\omega^2 R_0} + \left(7 - \frac{3\omega_0^2}{\omega^2}\right)\frac{\delta_{vis}}{4}\right], \tag{1.17a}$$

$$F_b^{(st)} = \frac{\pi\rho_0|A|^2 kR_0(1-\omega_0^2/\omega^2)\sin(2kd)}{(1-\omega_0^2/\omega^2)^2+\Delta^2}, \tag{1.17b}$$

where

$$\Delta = \delta_{rad} + \delta_{vis} + \frac{9(\tilde{\gamma}-1)\tilde{c}^2\tilde{\delta}_t}{2\lambda_\rho\omega^2 R_0^3}. \tag{1.18}$$

If we set $R_0/\tilde{\delta}_t \gg 1$ in Eq. (1.4) and drop the viscous terms in Eq. (1.17a), the resulting expressions will be identical. Thus, Eq. (1.17a) just refines Eq. (1.4) by including viscous effects, which, however, are not of vital importance in this case. Estimates show that the leading part belongs to thermal and radiation losses, as was correctly supposed by Yosioka and Kawasima [33]. If we set $R_0/\tilde{\delta}_t \gg 1$ in Eq. (1.7), it will turn into Eq. (1.17b). The fact that we have to pass to the limit $R_0/\tilde{\delta}_t \gg 1$ in Eqs. (1.4) and (1.7) in order to get Eqs. (1.17a) and (1.17b) does not mean, however, that Eqs. (1.4) and (1.7) are valid for arbitrary thermal effects. This follows from expressions obtained in [54] for the limit of strong dissipation:

$$F_b^{(tr)} = -\frac{\pi\rho_0|A|^2 kR_0(\Omega/\omega)^2(\delta_v/R_0)^2}{(\Omega/\omega)^4 + 4(\delta_v/R_0)^4}, \tag{1.19a}$$

$$F_b^{(st)} = -\pi\rho_0|A|^2 kR_0 \sin(2kd)\frac{(\Omega/\omega)^2 + (\delta_v/R_0)^4}{(\Omega/\omega)^4 + 4(\delta_v/R_0)^4}, \tag{1.19b}$$

where

$$\Omega = \left[\omega_0^2 - \frac{3(\tilde{\gamma}-1)\tilde{c}^2}{\tilde{\gamma}\lambda_\rho R_0^2}\right]^{1/2}. \tag{1.20}$$

Comparison of these equations with Eqs. (1.4) and (1.7) shows clearly that they cannot be obtained from Eqs. (1.4) and (1.7) by a limit passing. The reason is that Eqs. (1.4) and (1.7) ignore acoustic streaming, which is a key factor when $R_0 \ll \delta_v$. Peculiarities of bubble dynamics at strong dissipation, according to Eqs. (1.19a) and (1.19b), are that in a traveling wave field, bubbles move to the sound transducer, i.e., in the opposite direction with respect to the limit of weak dissipation, and in a standing wave field, they accumulate at the velocity nodes, similar to bubbles with $\omega_0 > \omega$ at weak dissipation and contrary to drops at strong dissipation.

Doinikov also examined viscous and thermal effects on the dynamics of a rigid sphere and a liquid drop in a diverging spherical wave field [52,53]. The behavior of a gas bubble in a diverging spherical wave was investigated taking account of viscous effects alone [56], and the case of elastic particle was not considered at all. However, the general, "viscous and thermal", theory, developed in [51], can easily be applied to these cases as well, if needed.

Some selected results of this section are summed up in Fig. 1. The figure shows the direction of motion of various particles in the limits of weak and strong dissipation except when the conditions that define the direction of the radiation force are too complicated.

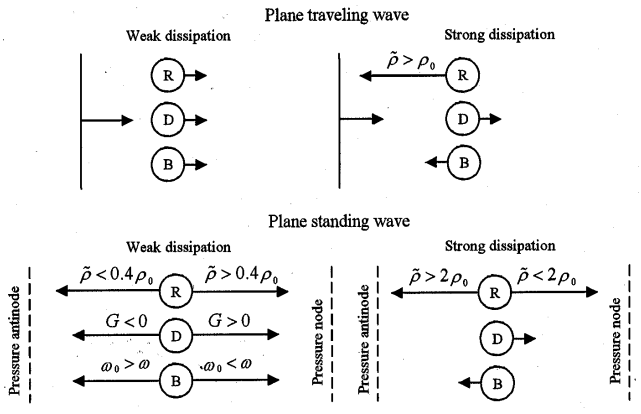

Figure 1. Motion of dispersed particles in the limits of weak and strong dissipation. R = rigid sphere, D = drop, B = bubble. $G = (5-2\lambda_\rho)/(2+\lambda_\rho) - \lambda_\rho c^2/\tilde{c}^2$.

2. Secondary forces

2.1. Interaction between two bubbles

The radiation interaction force between two pulsating bubbles is normally referred to as the *secondary Bjerknes force* after C.A. Bjerknes and his son V.F.K. Bjerknes, who were the first to investigate experimentally and theoretically this effect [13]. They derived an analytical expression for the above force, which can be represented as

$$F_B = \frac{2\pi\rho_0 |A|^2 R_{10} R_{20}}{L^2 \left(1-\omega_1^2/\omega^2\right)\left(1-\omega_2^2/\omega^2\right)}, \tag{2.1}$$

where R_{10} and R_{20} are the equilibrium bubble radii, L is the distance between the equilibrium centers of the bubbles, ω_1 and ω_2 are the fundamental resonance frequencies of the bubbles, and the other designations are the same as in § 1. $F_B > 0$ corresponds to the mutual attraction of the bubbles, while $F_B < 0$ to the mutual repulsion. Equation (2.1) shows that the repulsion occurs when ω lies between ω_1 and ω_2. Otherwise the bubbles attract each other. The Bjerknes theory is based on the following assumptions: (i) the surrounding medium is an ideal incompressible fluid; (ii) the gas within the bubbles obeys the adiabatic law; (iii) the spacing between the bubbles is much larger than their radii, $L \gg R_{10}, R_{20}$, so that the shape deviations of the bubbles from sphericity and the scattered waves of higher order than the primary ones can be neglected; (iv) the incident field is weak enough so that nonlinear oscillations are negligible. When these conditions are met, the Bjerknes theory is in agreement with experiments [57,58]. If, however, this is not the case, then effects are observed that cannot be explained by using Eq. (2.1). One such effect is the formation of stable bubble clusters known as *bubble grapes*, which were observed experimentally in [15] and [16]. The clusters consisted of several bubbles noticeably larger than resonance size. They neither coagulated nor broke down into individual bubbles as long as the sound field was on. An important point is that the sound field used in [15] was rather weak: The ratio of the driving pressure amplitude to the hydrostatic pressure did not exceed 0.035. (In [16], stronger fields were applied.) This fact suggests that the clusters are not associated with nonlinear bubble oscillations. The key to this problem was given by Zabolotskaya [59]. She has shown that Eq. (2.1) fails because of ignoring radiation coupling of the two bubbles, i.e., the influence of the bubbles' scattered fields on each other's pulsations. Allowing for this coupling (and the damping of the bubble pulsations) yields a refined formula for the interaction force

$$F_Z = \frac{2\pi\rho_0 |A|^2 R_{10} R_{20}}{L^2 |D|^2}\left[\left(\frac{\omega_1^2}{\omega^2}-1+\frac{R_{10}}{L}\right)\left(\frac{\omega_2^2}{\omega^2}-1+\frac{R_{20}}{L}\right)+\delta_1\delta_2\right], \tag{2.2}$$

where

$$D = \left(\omega_1^2/\omega^2 - 1 - i\delta_1\right)\left(\omega_2^2/\omega^2 - 1 - i\delta_2\right) - R_{10}R_{20}/L^2, \tag{2.3}$$

and δ_1 and δ_2 denote the total damping constants of the bubbles as defined in Eq. (1.7). Equation (2.2) shows that in fact the sign of the interaction force depends on the distance between the bubbles. In particular, if both bubbles are driven above resonance ($\omega > \omega_1, \omega_2$) and one (or both) of their resonance frequencies is close enough to ω, the interaction

force may change from attraction to repulsion as the bubbles come closer to each other. As a result, they can form a stable bound pair with a constant spacing. Obviously this effect provides an insight into the nature of the bubble grapes. The theory of Zabolotskaya was extended by Doinikov and Zavtrak [60,61], who developed an approach that allows for multiple re-scattering of sound between two bubbles and their shape oscillations and thereby makes it possible to calculate correctly the interaction force of the two bubbles down to very small separation distances. Using a different numerical approach, Pelekasis and Tsamopoulos [62,63] conducted extensive simulations of the relative motion of two bubbles in sound fields with relative driving pressure amplitudes of 0.2-0.3, allowing for shape deviations of the bubbles from sphericity. They also found that at small distances the attraction of the bubbles can change to repulsion if the bubbles are driven above resonance.

When the wavelength of sound λ_s is comparable to separation distances between bubbles, the compressibility of the host fluid is no longer negligible. This problem was first considered by Nemtsov [64]. He calculated the interaction force of two bubbles in an ideal compressible fluid subject to a plane traveling wave, assuming that $R_{10}, R_{20} \ll L, \lambda_s$, while kL is arbitrary. It turned out that (i) in addition to the Bjerknes term, Eq (2.1), inversely proportional to L^2, the interaction force involves a long-range term inversely proportional to L ; (ii) the force can change sign at large values of kL ; and (iii) the force on one bubble is not equal and opposite to that on the other bubble since in a compressible fluid a part of momentum is carried away by scattered waves to infinity. However, Nemtsov lost another long-range term of the interaction force, directed along the wave vector of the incident sound field. This error was corrected by Doinikov and Zavtrak [65]. Besides, they generalized Nemtsov's theory to sound fields of arbitrary geometry and took account of dissipative losses by incorporating the damping terms into the equations of radial bubble oscillations, as in [59]. As a result, provided the velocity potential of the incident field is specified by $\varphi_I = a(\boldsymbol{r})\exp(-i\omega t)$, the interaction force on the jth bubble (j=1,2) takes the form:

$$\boldsymbol{F}_j = \frac{2\pi\rho_0 R_{10}R_{20}}{|s_1|^2|s_2|^2}\,\mathrm{Re}\left\{a(\boldsymbol{r}_{3-j})\exp(ikL)\left[\frac{s_j s_{3-j}^* a^*(\boldsymbol{r}_j)\boldsymbol{e}_j}{L^2} - \frac{iks_j s_{3-j}^* a^*(\boldsymbol{r}_j)\boldsymbol{e}_j}{L} + \frac{s_1^* s_2^*}{L}\nabla_j a^*(\boldsymbol{r}_j)\right]\right\}, \tag{2.4}$$

where $s_j = \omega_j^2/\omega^2 - 1 - i\delta_j$, the asterisk denotes the complex conjugate, $\boldsymbol{e}_j = (\boldsymbol{r}_{3-j} - \boldsymbol{r}_j)/L$ is the unit vector directed from the jth bubble to the other bubble, and $\boldsymbol{r}_j$ is the position vector of the equilibrium center of the jth bubble. It is seen that the force $\boldsymbol{F}_j$ consists of three terms. The first term in square brackets is dominant in the limit $R_{10}, R_{20} \ll L \ll \lambda_s$ and turns to Eq. (2.2) for $kL \to 0$. The other two terms are long-range terms which owe their existence to the compressibility of the host fluid. The first of them is directed along the center line of the bubbles, while the second along the gradient of the incident field. The long-range terms prevail over the Bjerknes term at large values of kL. It can also be seen that owing to the factor $\exp(ikL)$ the force $\boldsymbol{F}_j$ is an alternating-sign function of L. Equation (2.4) was applied in [65] to a plane traveling wave, setting $a(\boldsymbol{r}) = A\exp(i\boldsymbol{k}\cdot\boldsymbol{r})$, and to a plane standing wave, setting $a(\boldsymbol{r}) = A\cos(\boldsymbol{k}\cdot\boldsymbol{r})$. Investigation of the relative motion of the bubbles revealed that in both cases the long-range terms can cause the bubbles to form bound pairs with a stable spacing on the order of the sound wavelength λ_s.

Consequences of abandoning another Bjerknes assumption were studied in [66,67]. This is the assumption of ideality of the host fluid. In [66,67], the interaction force between two spherical gas bubbles in a viscous incompressible liquid was calculated. All the other limitations of the Bjerknes theory, such as $R_{10}, R_{20} \ll L$, were kept. Account was taken of the translational oscillations of the bubbles, the vorticity of the linear scattered field, and acoustic streaming around the bubbles. Two types of boundary conditions at the bubble surface were considered: the boundary condition of adhesion of liquid particles to the bubble surface [66] and the boundary condition of slippage on the gas-liquid interface [67]. The following result was obtained:

$$\boldsymbol{F}_j = \frac{2\pi\rho_0 |A|^2 R_{10} R_{20}}{L^2 |D|^2} \boldsymbol{e}_j \left[(T_1 T_2 + \delta_1\delta_2)(1 + \mathrm{Re}\{\tau(z_j)\}) + \mathrm{Im}\{\tau(z_j)\}(\delta_j T_{3-j} - \delta_{3-j} T_j) \right], \tag{2.5}$$

where D is given by Eq. (2.3), $T_j = \omega_j^2/\omega^2 - 1 + R_{j0}/L$, $z_j = k_v R_{j0}$, $k_v = (1+i)/\delta_v$, and the function $\tau(z_j)$ is defined as

$$\tau(z_j) = \frac{(z_j^6 - 12 z_j^4)\exp(-iz_j) E_1(-iz_j) + 48 - 48 i z_j + 18 z_j^2 + 14 i z_j^3 - z_j^4 - i z_j^5}{16(z_j^2 + 9 i z_j - 9)} \tag{2.6a}$$

in the no-slip case, and

$$\tau(z_j) = \frac{z_j^6 \exp(-iz_j) E_1(-iz_j) - 36 + 36 i z_j + 12 z_j^2 - z_j^4 - i z_j^5}{z_j^2(18 - 18 i z_j - 3 z_j^2 + i z_j^3)} \tag{2.6b}$$

in the case of slippage, $E_1(z)$ denoting the integral exponent of the first order.

Comparison of Eq. (2.5) with Eq. (2.2) shows that agreement exists only in the limit of low viscosity, $R_{j0} \gg \delta_v$. If, however, $\delta_v \geq R_{j0}$, which occurs when the bubbles are small, or the driving frequency ω is low, or the viscosity of the host liquid is high, then there are essential discrepancies. In the no-slip case, Eq. (2.5) predicts a considerable decrease of the interaction force in magnitude. If slippage occurs, the force can even change sign, with respect to Eq. (2.2) and the no-slip case, provided the viscosity of the host liquid is high enough. This effect is illustrated in Fig. 2, adopted from [67], which presents a contour plot that shows the regions of attraction and repulsion for two air

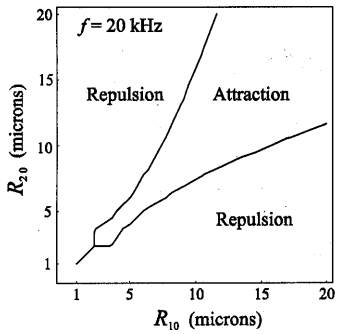

Figure 2. Regions of attraction and repulsion for two bubbles driven well below resonance in a high-viscosity liquid.

bubbles in glycerin in the range of bubble radii from 1 to 20 μm at the driving frequency $f = \omega/2\pi$ =20 kHz. In all cases the bubble pairs are driven far below resonance and therefore, according to the Bjerknes theory, the bubbles should undergo mutual attraction. However, Fig. 2 displays that strong viscous effects can give rise to quite large areas of repulsion in the parametric space.

2.2. Interaction between a bubble and a solid particle

Interest in the interaction of gas bubbles with solid particles in a sound field is aroused by applications in acoustic flotation [7,68,69] and medical ultrasonics [8,70,71]. In [8], the force induced by an acoustically driven bubble on a solid spherical particle is specified by

$$\boldsymbol{F}_p = \frac{4\pi\rho_0|A|^2 R_{b0}^2 R_p^3}{L^5\left[(1-\omega_{b0}^2/\omega^2)^2+\delta_b^2\right]}\left(\frac{\rho_p-\rho_0}{\rho_0+2\rho_p}\right)\boldsymbol{e}_p, \tag{2.7}$$

where R_{b0} is the equilibrium radius of the bubble, R_p the radius of the solid particle, ω_{b0} the monopole resonance frequency of the bubble, δ_b the damping constant of the bubble, ρ_p the density of the particle, $\boldsymbol{e}_p$ the unit vector directed from the equilibrium center of the particle to that of the bubble (see Fig. 3), and the other designations are the same as in the preceding subsection. Equation (2.7) is based on the same assumptions as Eq. (2.1), namely, $R_{b0}, R_p \ll L$, the surrounding liquid is ideal and incompressible, etc. According to Eq. (2.7), particles denser than the host liquid are attracted by the bubble, while particles less dense than the host liquid are repelled by it.

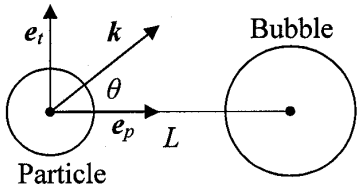

Figure 3. Geometry of the system in the case of interaction between a gas bubble and a solid particle.

Equation (2.7) implies that the oscillations of the particle are induced by the scattered field of the bubble alone. If, however, we take into account that the incident sound field by itself causes the particle to oscillate as well, then we get [68]

$$\boldsymbol{F}_p = (2/3)\pi R_p^3 R_{b0}^2(\rho_p-\rho_0)L^{-3}\,\mathrm{Re}\left\{\dot{R}_b^*\left[\boldsymbol{U}_p - 3(\boldsymbol{e}_p\cdot\boldsymbol{U}_p)\boldsymbol{e}_p\right]\right\}, \tag{2.8}$$

where $\dot{R}_b$ is the velocity of the radial pulsations of the bubble, the overdot denotes the time derivative, and $\boldsymbol{U}_p$ is the absolute translational velocity of the particle. By virtue of the assumption that $R_{b0}, R_p \ll L$, $\dot{R}_b$ can be taken as

$$\dot{R}_b = \varphi_I(\boldsymbol{r}_b)\left[R_{b0}\left(1-\omega_{b0}^2/\omega^2+i\delta_b\right)\right]^{-1}, \tag{2.9}$$

where $\varphi_I(\boldsymbol{r})$ is the incident velocity potential, and $\boldsymbol{r}_b$ is the position vector of the bubble center. The particle velocity $\boldsymbol{U}_p$ is defined by the well-known formula [72]

$$\boldsymbol{U}_p = 3\boldsymbol{v}\rho_0/(\rho_0 + 2\rho_p), \tag{2.10}$$

where $\boldsymbol{v}$ is the liquid velocity at the location of the particle as if the particle were absent. This velocity can be divided into two parts: $\boldsymbol{v} = \boldsymbol{v}_I + \boldsymbol{v}_b$, where $\boldsymbol{v}_I$ is generated directly by the incident field and $\boldsymbol{v}_b$ is due to the scattered field of the bubble. Within the stipulated limits, $\boldsymbol{v}_b$ is given by $\boldsymbol{v}_b = -R_{b0}^2\dot{R}_b\boldsymbol{e}_p/L^2$. It is easy to check that, if we neglect $\boldsymbol{v}_I$ and set $\varphi_I(\boldsymbol{r}) = A\exp(-i\omega t)$, Eq. (2.8) reduces to Eq. (2.7).

In reality, however, $\boldsymbol{v}_I$ always exists and therefore, in addition to the component directed along the center line of the bubble and the particle, the force has a component along the wave vector of the incident field. For a plane traveling wave, putting $\varphi_I(\boldsymbol{r}) = A\exp(i\boldsymbol{k}\cdot\boldsymbol{r} - i\omega t)$, neglecting $\boldsymbol{v}_b$ and assuming $kL \ll 1$, Eq. (2.8) yields

$$\boldsymbol{F}_p^{(tr)} = 2B\delta_b L^{-3}\left[3(\boldsymbol{e}_p\cdot\boldsymbol{e}_k)\boldsymbol{e}_p - \boldsymbol{e}_k\right] = F_{pL}\boldsymbol{e}_p + F_{pt}\boldsymbol{e}_t, \tag{2.11}$$

where

$$B = \frac{\pi\rho_0|A|^2 R_{b0}R_p^3(\rho_p - \rho_0)k}{(\rho_0 + 2\rho_p)\left[(1-\omega_{b0}^2/\omega^2)^2 + \delta_b^2\right]}, \tag{2.12}$$

$$F_{pL} = 4B\delta_b L^{-3}\cos\theta, \qquad F_{pt} = -2B\delta_b L^{-3}\sin\theta, \tag{2.13}$$

$\boldsymbol{e}_k = \boldsymbol{k}/k$, $\boldsymbol{e}_t$ is the unit vector $\perp$ $\boldsymbol{e}_p$, F_{pL} is the force component along the center line, F_{pt} is the tangential component perpendicular to the center line, and θ is the angle between the vectors $\boldsymbol{e}_p$ and $\boldsymbol{k}$, see Fig. 3. The interaction between a bubble and a heavy particle ($\rho_p > \rho_0$) at various angles θ is shown in Fig. 4. Note that the tangential component of the force tends to bring the particle to the region of attraction, which corresponds to $\theta < \pi/2$.

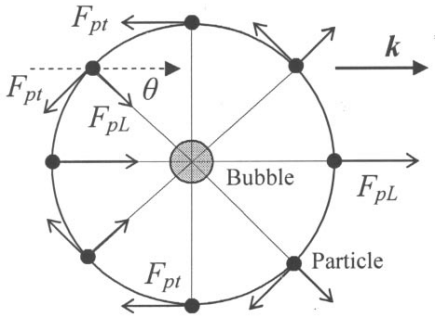

Figure 4. Interaction between a bubble and a heavy solid particle in a plane traveling wave at various angles θ.

For a plane standing wave, setting $\varphi_I(\boldsymbol{r}) = A\cos(\boldsymbol{k}\cdot\boldsymbol{r})\exp(-i\omega t)$, one finds

$$\boldsymbol{F}_p^{(st)} = B(1-\omega_{b0}^2/\omega^2)\sin(2\boldsymbol{k}\cdot\boldsymbol{r}_0)L^{-3}\left[3(\boldsymbol{e}_p\cdot\boldsymbol{e}_k)\boldsymbol{e}_p - \boldsymbol{e}_k\right] = F_{pL}\boldsymbol{e}_p + F_{pt}\boldsymbol{e}_t, \tag{2.14}$$

where F_{pL} and F_{pt} are now given by

$$F_{pL} = 2B(1-\omega_{b0}^2/\omega^2)\sin(2\boldsymbol{k}\cdot\boldsymbol{r}_0)L^{-3}\cos\theta, \qquad F_{pt} = -B(1-\omega_{b0}^2/\omega^2)\sin(2\boldsymbol{k}\cdot\boldsymbol{r}_0)L^{-3}\sin\theta. \tag{2.15}$$

The vector $\boldsymbol{r}_0$ designates the location of the bubble-particle pair in the wave field. The difference between $\boldsymbol{r}_b$ and $\boldsymbol{r}_p$ can be neglected since $kL \ll 1$. It is seen that in the case of a standing wave, the sign of the force is also dependent on the ratio ω_{b0}/ω and the sign of $\sin(2\boldsymbol{k}\cdot\boldsymbol{r}_0)$. Positive values of $\sin(2\boldsymbol{k}\cdot\boldsymbol{r}_0)$ mean that the bubble-particle pair is to the right of the nearest pressure antinode in the direction of wave propagation and vice versa. Thus, in the case of a plane standing wave, Fig. 4 would show the interaction between a heavy particle and a bubble which are to the right of the pressure antinode, the bubble being driven above resonance ($\omega_{b0} < \omega$).

Equations (2.11) and (2.14) can be considered as a first approximation to Eq. (2.7) that allows for the compressibility of the host liquid. They are of higher (first) order in kR_{b0} but of lower (third) order in R_{b0}/L. In [68], terms of the order $(kR_{b0})^2(R_{b0}/L)^2$ are also derived. Clearly we deal here with the same situation as in the case of two bubbles in a compressible liquid: Allowing for the liquid compressibility gives rise to long-range force terms the last of which should be inversely proportional to L.

The liquid compressibility and the long-range force terms are of importance at large separation distances. At small distances, however, other effects are dominant, namely, multiple re-scattering of sound between the bubble and the particle and the shape oscillations of the bubble. In this case, Eq. (27) is not a good approximation either, because it only takes account of the primary scattered wave from the bubble and absolutely ignores the effect of the particle on the bubble oscillations. In [73], an approach is proposed that allows for all the above processes and thus makes possible a correct calculation of the radiation interaction force between a bubble and a solid particle for small separations. The force is obtained as an infinite series, terms of which are calculated from re-currence formulas with any accuracy required. It can also be said that the force is expanded in a power series in $R_p/L < 1$ and then a procedure is applied that enables one to evaluate the coefficients of the series at any powers of R_p/L. Numerical investigations made in [73] show that at small separations the interaction force can differ from Eq. (2.7) both in magnitude and in sign. In particular, the force on a heavy particle is found to change from attraction to repulsion if the driving frequency is slightly above some of the natural frequencies of the bubble shape modes.

2.3. Interaction between a bubble and a liquid drop

The study of the radiation interaction between a gas bubble and a liquid drop is mainly of biomedical interest. In biomedical ultrasonics, one has to deal with the radiation forces exerted by pulsating gas bubbles on the components of blood plasma [8,70,71]. A detailed knowledge of this process is important for the efficient and safe use of ultrasound in medical applications. In this context, one might expect that a liquid drop is a better approximation for the blood components than a rigid sphere.

When the distance between a bubble and a drop is so much larger than their sizes that their shape oscillations are negligible, the interaction force between the bubble and the drop can by approximated by Eq. (2.8) [or by Eq. (2.7) if $(R_{b0}/L)^2 \gg kR_{b0}$]. For small separations, however, the shape oscillations are no longer negligible, especially if their natural frequencies are close to the driving frequency, and should be taken into account. This problem was first examined in [74]. Just as in [73], the interaction force of a bubble and a drop is expressed as an infinite series, terms of which are calculated by means of recurrence formulas. All the assumptions accepted in [73] are valid in [74] as well, except that the medium inside the drop is taken to be an ideal incompressible liquid. Thus, the compressibility of the drop is still ignored but its shape oscillations are allowed for. It is shown by numerical examples that the pattern of the radiation interaction between a bubble and a drop, when they are close to each other, is quite complex, especially if the driving frequency lies close to the natural frequencies of the shape modes of the bubble or the drop. In this case, the behavior of the interaction force has the following typical features: As the separation between the bubble and the drop is reduced, the interaction force, first, increases in magnitude much faster than Eq. (2.7) predicts, and second, can change sign. In the case of a light drop, i.e., a drop less dense than the host liquid, the interaction force changes from repulsion to attraction. It follows that light drops can be trapped by gas bubbles if they, due to some forces that counteract the radiation interaction force, are brought close enough together. For a heavy drop, denser than the host liquid, the interaction force changes from attraction to repulsion. Thus, heavy drops and gas bubbles can form stable structures in a sound field, in which separations between the particles remain constant as long as the sound is on. Numerical calculations also show that there are situations where the interaction force between a bubble and a heavy drop changes sign twice, becoming again attractive when they are brought even closer together.

2.4. Interaction between two rigid spheres

As already pointed out, an analytical expression for the interaction force of two rigid spheres was first derived by König [14]. In the case that the spheres are set in motion by a sound field, König's result can be represented as [75]

$$\boldsymbol{F}_j = \frac{3\pi\rho_0 R_1^3 R_2^3}{L^4}\left\langle \boldsymbol{U}_1(\boldsymbol{U}_2\cdot\boldsymbol{e}_j)+\boldsymbol{U}_2(\boldsymbol{U}_1\cdot\boldsymbol{e}_j)+\boldsymbol{e}_j(\boldsymbol{U}_1\cdot\boldsymbol{U}_2)-5\boldsymbol{e}_j(\boldsymbol{U}_1\cdot\boldsymbol{e}_j)(\boldsymbol{U}_2\cdot\boldsymbol{e}_j)\right\rangle, \tag{2.16}$$

where $\boldsymbol{F}_j$ is the force on sphere j (j=1,2), R_j the radius of sphere j, $\boldsymbol{e}_j$ the unit vector directed from the equilibrium center of sphere j to that of the other sphere, $\langle\ \rangle$ denotes an average over time, and $\boldsymbol{U}_j$ is the velocity of sphere j relative to the velocity of the host fluid, which is specified by $\boldsymbol{U}_j = 2(\rho_0-\rho_j)\boldsymbol{v}_I(\boldsymbol{r}_j)/(\rho_0+2\rho_j)$, where ρ_j is the density of sphere j, and $\boldsymbol{v}_I(\boldsymbol{r}_j)$ denotes the fluid velocity generated by the incident sound field in the position of sphere j as if both spheres were absent. Note also that Eq. (2.16) is valid on condition that $R_1, R_2 \ll L \ll \lambda_s$.

For a plane traveling wave, with $\varphi_I(\boldsymbol{r}) = A\exp(i\boldsymbol{k}\cdot\boldsymbol{r}-i\omega t)$, Eq. (2.16) gives

$$\boldsymbol{F}_j^{(tr)} = CL^{-4}\left[2(\boldsymbol{e}_j\cdot\boldsymbol{e}_k)\boldsymbol{e}_k+\left(1-5(\boldsymbol{e}_j\cdot\boldsymbol{e}_k)^2\right)\boldsymbol{e}_j\right] = F_{Lj}\boldsymbol{e}_j + F_{tj}\boldsymbol{e}_{tj}, \tag{2.17}$$

where

$$C = \frac{6\pi\rho_0 |A|^2 k^2 R_1^3 R_2^3 (\rho_1 - \rho_0)(\rho_2 - \rho_0)}{(\rho_0 + 2\rho_1)(\rho_0 + 2\rho_2)}, \tag{2.18}$$

$$F_{Lj} = CL^{-4}\left(1 - 3\cos^2\theta_j\right), \qquad F_{tj} = CL^{-4}\sin 2\theta_j, \tag{2.19}$$

$\cos\theta_j = \boldsymbol{e}_j \cdot \boldsymbol{e}_k$, and $\boldsymbol{e}_{tj} \perp \boldsymbol{e}_j$. Figure 5 shows the directions of the longitudinal and the tangential components of the interaction force for various angles between the wavevector and the center line of the spheres. The densities of both spheres are assumed to be higher (or lower) than the density of the host fluid. According to Eqs. (2.19), the changeover of the longitudinal force from repulsion to attraction occurs when $\cos\theta_1 = 1/\sqrt{3}$ ($\theta_1 \approx 55^\circ$), and the tangential force is always directed toward the region of attraction.

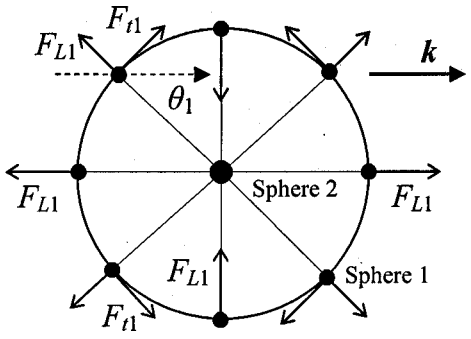

Figure 5. Interaction between two rigid spheres in a plane traveling wave.

Doinikov and Zavtrak [76] extended König's theory to compressible fluids. They assumed that (i) $R_1, R_2 \ll L, \lambda_s$; (ii) the ratio of L to λ_s is arbitrary; (iii) the spheres oscillate independently of each other but with the same frequency. Their study revealed that, first, in addition to Eq. (2.16), the interaction force involves three more long-range terms, which are inversely proportional to L^3, L^2, and L. Second, all of the four force terms depend on the re-scattering phase kL, which is to say that the sign of the force oscillates with increasing L.

Another shortcoming of Eq. (2.16) is that it ignores dissipative effects. There are experimental data that, when subjected to a sound field, aerosol particles in air in the regime of Stokes flow behave inversely with respect to what is predicted in Fig. 5: They attract each other at $\theta_j = 0$ and repel each other at $\theta_j = \pi/2$ [7]. In the light of these observations, the question of how dissipative processes alter the expression for the radiation interaction force between rigid spheres is of great interest. This issue still remains open.

2.5. Interaction between *N* compressible spheres in a compressible fluid

All the studies described in this section so far have two main flaws. First, all of them are concerned only with pairwise interactions of particles, whereas in practice we have normally to deal with multi-particle populations. Second, none of them proposes a theory that would allow us to calculate the interaction force for arbitrary separation distances. In the case of two bubbles, say, Eq. (2.4) allows us to evaluate the interaction force at large and intermediate distances, Eqs. (2.1) and (2.2) are good for intermediate distances, and the approach developed in [60] provides the force at intermediate and small distances. However, none of them is valid for all distances. In other words, none of them allows us to trace the interaction between two bubbles continuously from large to small separations. There are also other flaws. For example, each of the expressions presented in the preceding subsections is only valid for that particle pair for which it was derived. We cannot, for instance, obtain the interaction force of a bubble and a solid particle from the formula for two bubbles and vice versa. An expression for the interaction force of a solid particle and a liquid drop (or of two drops) is absent at all, although it is evident that under certain conditions, these cases should manifest specific features, and so on. In other words, the above studies do not provide a general theory that would be valid for particle pairs of any nature, for any separations, and what is more, for an arbitrary number of particles.

An attempt to develop such a theory was recently made by Doinikov [77]. He used the following assumptions: (i) N particles (bubbles, drops, their mixture, etc.) are freely suspended in a fluid irradiated by an acoustic wave field; (ii) the media outside and inside the particles are ideal compressible fluids subject to the Euler equation; (iii) the particles are spherical at rest; (iv) the incident field is moderate so that the scattered (outside) and refracted (inside) fields of the particles can be taken in linear approximation; (v) the system is in a steady state, in which the particles oscillate with the driving frequency alone; (vi) no restrictions are imposed on the radii of the particles, the separations between them, and the wavelength of sound outside and inside the particles; (vii) shape modes of all orders and multiple re-scattering of sound between the particles are allowed for. The purpose of the research was to derive an analytical expression, accurate to the second order in the acoustic pressure amplitude, for the time-averaged radiation force experienced by an arbitrary particle of the system. The expression was obtained in the form of an infinite series, terms of which are some known functions of the system parameters multiplied by the so-called linear scattering coefficients. These latter specify the linear scattered field of the particle in hand and are calculated from a set of equations, which is also derived in [77]. Thus, the calculation of the acoustic radiation forces acting in the system of particles of interest is reduced to the calculation of the linear scattering coefficients of the particles.

To gain a clearer idea of the theory developed in [77], let us consider results obtained there for the system of two particles. The geometry of the system is shown in Fig. 6. In the case of two particles, the expression for the radiation force on the jth particle (j=1,2) takes the form

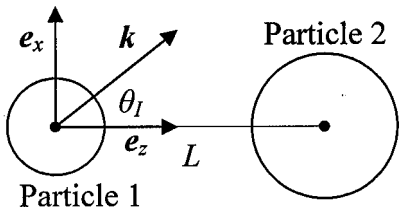

Figure 6. Notation used in [77] in the case of two particles.

$$\begin{aligned} \boldsymbol{F}_j = \rho_0 \,\mathrm{Re} \sum_{n=0}^{\infty} \sum_{m=-n}^{n} D_n^{(j)} B_{nm}^{(j)} \Big\{ & 2\sqrt{(n+1)^2 - m^2}\, B_{(n+1)m}^{(j)*} \boldsymbol{e}_z \\ & + \Big[\sqrt{(n-m+1)(n-m+2)}\, B_{(n+1)(m-1)}^{(j)*} \\ & - \sqrt{(n+m+1)(n+m+2)}\, B_{(n+1)(m+1)}^{(j)*} \Big] \boldsymbol{e}_x \Big\}. \end{aligned} \tag{2.20}$$

Here, $D_n^{(j)}$ are known quantities (explicit expressions for them are given in [77]), and $B_{nm}^{(j)}$ are the above-mentioned linear scattering coefficients, which are calculated from the following set of equations:

$$B_{nm}^{(j)} + Q_n^{(j)} \sum_{l=|m|}^{\infty} K_{nml}^{(j)} B_{lm}^{(3-j)} = -Q_n^{(j)} A_{nm}^{(j)}, \tag{2.21}$$

where $Q_n^{(j)}$ are known functions of the system parameters, $K_{nml}^{(j)}$ are known quantities, too, which are expressed in terms of the Clebsch-Gordan coefficients, and $A_{nm}^{(j)}$ are the multipole coefficients responsible for the type of incident field, which are also assumed to be known. For example, in the case of a plane traveling wave, they are specified by

$$A_{nm}^{(1)} = 4\pi A i^n Y_{nm}^*(\theta_I, 0), \qquad A_{nm}^{(2)} = \exp(ikL\cos\theta_I) A_{nm}^{(1)}, \tag{2.22}$$

where A is the complex amplitude of the incident potential, $Y_{nm}(\theta,\varepsilon)$ is the spherical harmonic, and θ_I is the angle between the vectors $\boldsymbol{k}$ and $\boldsymbol{e}_z$, see Fig. 6. It should be noted that Eq. (2.20) involves both the primary and the secondary radiation forces. This equation also shows that the main point in calculating the forces is the calculation of the coefficients $B_{nm}^{(j)}$ from the set of equations (2.21). If this task is solved, then the radiation forces can easily be found for any values of the system parameters with any accuracy required.

Figure 7, adopted from [77], exemplifies the interaction between two air bubbles (R_{10} = 50 μm, R_{20} = 35 μm) in water subject to a plane traveling wave field. The evolution of this interaction from large to small separations was followed by using Eqs. (2.20) – (2.22). It is assumed that the traveling wave is propagating from left to right along the center line of the bubbles, which are driven in such a way that the monopole resonance frequency of the smaller bubble is not much below the driving frequency f = 100 kHz. Figure 7 displays the normalized (divided by $|A|^2$) interaction force on the left-hand bubble versus the dimensionless separation distance defined as $D = L/(R_{10} + R_{20})$.

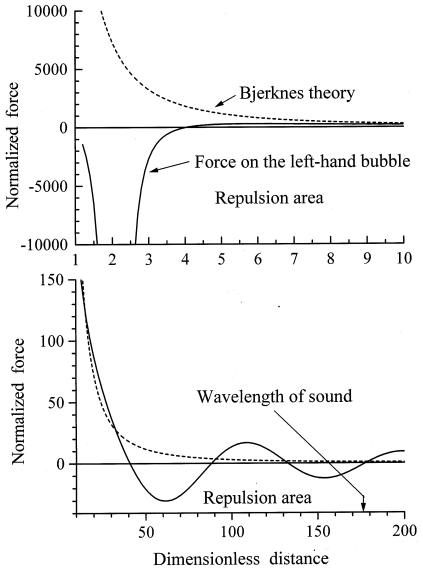

Figure 7. Interaction force of two bubbles driven above resonance as a function of separation distance. The forcing is a plane traveling wave propagating along the center line of the bubbles from the left to the right.

Shown dotted are predictions of the Bjerknes theory, Eq. (2.1). The solid curve presents the force that is obtained from Eq. (2.20) minus the primary radiation force, which is calculated from Eq. (1.3a). One can see that, as already pointed out, the Bjerknes theory is only valid for intermediate separations. For small separations, the upper part of Fig. 7, the Bjerknes theory predicts mutual attraction and coalescence of the bubbles. In fact, the interaction force changes sign and thus keeps the bubbles from coalescing. For large separations, the lower part of Fig. 7, the Bjerknes theory predicts only a rapid decrease of the interaction force in magnitude. What actually happens is that the sign of the force oscillates, which is a consequence of the finite compressibility of the host liquid. Note also that the value of D for which the first sign reversal is observed is quite small compared to the value of D corresponding to the sound wavelength in the host liquid. That is to say, the liquid compressibility manifests itself at distances even smaller than half the sound wavelength.

Figure 8 illustrates more realistic cases, which were simulated in [77], where the wavevector does not coincide with the center line of two bubbles. The figure shows trajectories of the time-averaged translational motion of two air bubbles in water subject to a plane traveling wave. It is assumed that the sound wave first reaches the left-hand bubble, the driving frequency f= 130 kHz, and the acoustic pressure amplitude is 0.1 bar. The x- and y-axes of Fig. 8 are marked in terms of dimensionless units of length that are defined as $D = d/(R_{10} + R_{20})$, where d is dimensional distance. The arrows next to the curves indicate the direction of bubble motion. Shown dashed are predictions of the Bjerknes theory, which are obtained from Eqs. (2.1) and (1.3a). In Fig. 8(a), the initial

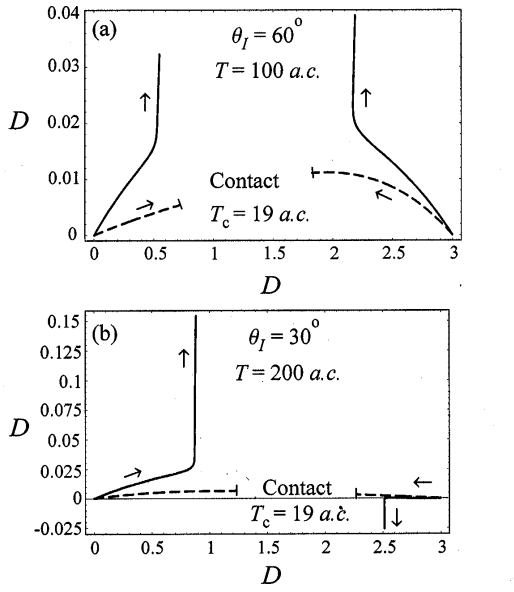

Figure 8. Trajectories of the time-averaged translational motion of two interacting bubbles in a plane traveling wave.

angle between the wavevector and the center line of the bubbles is $\theta_I = \pi/3$, the mean bubble radii are R_{10} = 50 μm and R_{20} = 30 μm (both bubbles are driven above resonance), and the temporal interval of computation T is 100 a.c. (acoustic cycles). One can see that the bubbles are initially attracted to each other, slowly moving in the direction of wave propagation. According to the Bjerknes theory, they come into contact (and then probably coalesce) within the interval T_c =19 a.c. The improved theory shows, however, that the interaction force becomes repulsive at small separations, as in Fig. 7, and the bubbles stop approaching. Figure 8(*b*) shows the same bubble pair but at $\theta_I = \pi/6$ and over T = 200 a.c. In addition, the bubbles swap places, i.e., the smaller bubble is now on the left. The pattern of motion is substantially changed. It may be suggested that the *y*-component of the interaction force counteracts the primary radiation force on the right-hand bubble and causes it to move against the sound wave. These two examples demonstrate that the angle of sound incidence can be of crucial importance in bubble interactions.

In conclusion, it should be emphasized once again that, although the examples presented here (and in [77]) are concerned only with two bubbles, Eq. (2.20) is valid for any pairs of particles. In particular, all the results presented in §§ 2.1 – 2.4, except for Eq. (2.5) which is based on the model of viscous fluid, can be obtained from Eq. (2.20) by setting appropriate parameters for the inside media of two particles at issue. In the case of multi-particle interactions, a more general formula from [77] should be applied instead of Eq. (2.20). The only limitation on the number of interacting particles is the power of your computer.

3. Radiation forces in strong fields

So far we have dealt with the theory of acoustic radiation forces for weak fields, where these forces are treated as a weakly nonlinear effect quadratic in the acoustic forcing amplitude. In other words, all the expressions for the radiation forces presented above are just leading terms of the series expansions of "exact" forces in the amplitude of the acoustic driving pressure p_a , which is assumed to be small compared to the hydrostatic pressure p_0 in the host fluid, $P_a/P_0 \ll 1$. This theory will be called further *linear theory* since it takes account of only linear oscillations of particles. Experiments show that in strong sound fields, with pressure amplitudes on the order of or higher than p_0, bubble dynamics does not always follow the linear theory. For example, bubbles execute erratic "dancing" motions in standing waves of high intensity [78], form a halo around the central pressure antinode in acoustic resonators [79], group themselves into branched filamentary structures known as *acoustic streamers* [9,18], etc. The linear theory cannot explain such phenomena because of their evident nonlinear nature.

Akhatov *et al*. [80] were the first to investigate the primary radiation force on a bubble in a strong acoustic field. It is known that the hydrodynamic force on a small body in an ideal fluid can be written as [72]

$$\boldsymbol{F} = -\int_S p\boldsymbol{n}dS = -\int_V \boldsymbol{\nabla} p dV \approx -V\boldsymbol{\nabla} p. \tag{3.1}$$

Here, S is the surface of the body, $\boldsymbol{n}$ is the outward normal to S , p is the pressure in the ambient fluid, and V is the volume of the body. If p and V vary periodically in time, the net force on the body is the time average of $\boldsymbol{F}$. Thus, the primary radiation force on a small spherical bubble in a sound wave field can be represented as

$$\boldsymbol{F}_{pr} = -\frac{4}{3}\pi \left\langle R^3(t)\boldsymbol{\nabla} p_{ex}(t)\right\rangle, \tag{3.2}$$

where $p_{ex}(t)$ is the incident sound pressure. The time-varying radius of the bubble *R(t)* can be calculated using the Keller-Miksis model [81]:

$$\left(1-\frac{\dot{R}}{c}\right)R\ddot{R}+\left(\frac{3}{2}-\frac{\dot{R}}{2c}\right)\dot{R}^2 = \left(1+\frac{\dot{R}}{c}\right)\frac{p_s}{\rho_0}+\frac{R}{\rho_0 c}\frac{dp_s}{dt}, \tag{3.3}$$

where

$$p_s = \left(P_0+\frac{2\sigma}{R_0}\right)\left(\frac{R_0}{R}\right)^{3\tilde{\gamma}}-\frac{2\sigma}{R}-\frac{4\eta\dot{R}}{R}-P_0-p_{ex}(t), \tag{3.4}$$

and the other designations have the same meaning as in the preceding sections. These equations make possible a numerical investigation of the primary radiation force acting on a small bubble in a strong acoustic field. It is this approach that was used by Akhatov *et al.* in [80]. They assumed that the external sound field $p_{ex}(t)$ is a standing spherical wave and the bubble is in the close vicinity of the pressure antinode, in the center of which the acoustic pressure is specified by $p_a(t) = -P_a \sin\omega t$, the amplitude P_a exceeding 1 bar. It was found that in a strong field there is a threshold value of the equilibrium bubble radius, known as *dynamical Blake threshold* [82], which is typically equal to a few microns, such that smaller bubbles are trapped in the pressure antinode, while bigger

bubbles are repelled from it. This result is in contrast to predictions of the linear theory since in both cases bubbles are driven far below resonance. It gives an insight into the mechanism of the bubble halos which are formed near pressure antinodes in resonator cells under high-intensity acoustic driving [79].

Using the same approach as in [80], Doinikov [83] investigated the primary force acting on a small bubble in a strong acoustic field in the presence of another bubble. His results show that neighboring bubbles very substantially affect each other's primary radiation forces even if separation distances between them are large compared with their size. The effect is built up with increasing acoustic pressure amplitude. As a consequence, the peculiar features of the primary forces in strong fields, which were found in [80], such as the changeover from attraction to repulsion with increasing driving pressure amplitude, manifest themselves earlier and more vigorously.

In [80,83], inferences about the bubble behavior in a strong field are made on the basis of examination of acoustic radiation forces, which are time-averaged quantities. A different approach is advanced in [84,85]. The radiation forces are not calculated. Instead, a set of equations is derived and then solved numerically that allows one to trace instantaneous translational motion of a bubble. In [85], which is an extension of [84], using the Lagrangian formalism, the following equations are obtained:

$$\left(1-\frac{\dot{R}}{c}\right)R\ddot{R}+\left(\frac{3}{2}-\frac{\dot{R}}{2c}\right)\dot{R}^2-\left(1+\frac{\dot{R}}{c}\right)\frac{p_s}{\rho_0}-\frac{R}{\rho_0 c}\frac{dp_s}{dt}-\frac{\dot{x}^2}{4}=0, \tag{3.5}$$

$$\ddot{x}+\frac{3\dot{R}\dot{x}}{R}=\frac{3F_{ex}}{2\pi\rho_0 R^3}, \tag{3.6}$$

where p_s is given by Eq. (3.4), $x(t)$ is the instantaneous position of the center of the bubble, and F_{ex} denotes external forces on the bubble, such as the primary radiation force, given by Eq. (3.2), and the Levich viscous drag [86]. Equation (3.5) governs the radial pulsations of the bubble and Eq. (3.6) its translational motion. Solving these equations numerically, one can get the position of the bubble *x(t)* for any moment of time and plot its path in the sound field. Figure 9 gives examples of such paths for air bubbles in water. It is assumed that the forcing is a plane standing wave with a driving frequency of 25 kHz and a pressure amplitude P_a. The bubble position is depicted in terms of a normalized distance from the pressure antinode. This distance is defined as $x(t)/\lambda_s$. The position zero of the *y* axis corresponds to the pressure antinode, 0.25 to the pressure node, 0.5 to the next antinode, and so forth. Figure 9(*a*) shows the translational motion of a bubble driven above resonance. One can see that, following the linear theory, the bubble moves to the pressure node and oscillates about it with damped amplitude. The behavior of a bubble driven below resonance, shown in Fig. 9(*b*), does not comply with the linear theory: Instead of moving to the pressure antinode, the bubble reciprocates about the pressure node. This result is of interest in the context of the so-called *dancing motion*, which is demonstrated by bubbles in high-intensity standing waves [78]. It is generally agreed that the dancing motion is caused by the presence of shape oscillations that are parametrically excited by the bubble pulsations when the driving pressure amplitude exceeds a threshold. Since the thresholds for the onset of shape oscillations are noticeably lower than the values of P_a for which the effect shown

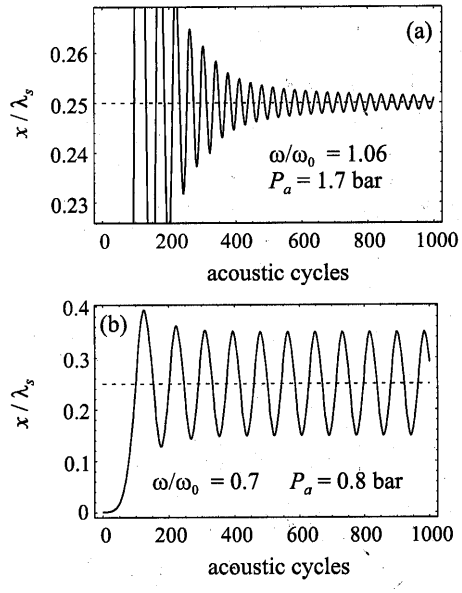

Figure 9. Translational motion of a bubble driven (*a*) above resonance and (*b*) below resonance in a plane standing wave of high intensity.

in Fig. 9(*b*) appears, there is no doubt that the shape oscillations are the primary source of the dancing motion. Nevertheless, it is of interest to notice that a spherical bubble, not undergoing shape distortions, can also execute irregular translational motions in a standing wave field if its intensity is high enough.

Let us now turn to secondary radiation forces. Using a peculiar approach, Oguz and Prosperetti [87] investigated numerically the interaction of two bubbles, maintaining all the restrictions of the Bjerknes theory but assuming that the bubbles oscillate slightly nonlinearly. They found that nonlinear effects can change the sign of the interaction force with respect to the predictions of Eq. (2.1). In particular, repulsion may also appear even if both of the bubbles are driven below their fundamental resonance frequencies ω_1 and ω_2. It was observed that the repulsive force emerged if twice the driving frequency 2ω lay between ω_1 and ω_2 and the forcing was high enough, on the order of 0.5 bar at a static pressure of 1 bar. For lower driving pressures and other relations between the frequencies the effect disappeared. Oguz and Prosperetti conjectured that it was caused by a strong component at twice the driving frequency developing in the bubble pulsations due to the strong forcing. This hypothesis was verified by Doinikov [88]. He obtained an analytical expression for the interaction force between two bubbles accurate up to a component induced by the second harmonic of the bubble oscillations and showed that this component can prevent the bubbles from coalescing, causing them either to repel each other or to form a bound pair with some stable separation. This occurs providing the imposed sound field is strong enough so that the second-harmonic force component is comparable to the "linear" component of the interaction force, given by Eq. (2.1).

Extending the approach suggested in [80] to the case of two bubbles, Mettin *et al*. [89] investigated numerically the time-averaged interbubble force in strong fields with pressure amplitudes exceeding 1 bar. Applying Eq. (3.1) to two bubbles, they represented the force of the first bubble on the second one as

$$\boldsymbol{F}_2 = -\left\langle V_2 \boldsymbol{\nabla} p_1\big|_{r=L} \right\rangle, \tag{3.7}$$

where $V_2 = 4\pi R_2^3/3$ is the time-varying volume of the second bubble, and p_1 is the scattered pressure of the first bubble, given by

$$p_1 = \frac{\rho_0}{r}\frac{d}{dt}\left(R_1^2 \dot{R}_1\right). \tag{3.8}$$

For calculation of the bubble radii, they generalized Eq. (3.3) to the case of two interacting bubbles by incorporating terms that allow for radiation coupling between the bubbles, i.e., the influence of the bubbles' scattered fields on each other's pulsations:

$$\left(1-\frac{\dot{R}_j}{c}\right)R_j\ddot{R}_j + \left(\frac{3}{2}-\frac{\dot{R}_j}{2c}\right)\dot{R}_j^2 = \left(1+\frac{\dot{R}_j}{c}\right)\frac{p_{sj}}{\rho_0} + \frac{R_j}{\rho_0 c}\frac{dp_{sj}}{dt} - \frac{1}{L}\frac{d}{dt}\left(\dot{R}_{3-j}R_{3-j}^2\right). \tag{3.9}$$

Here, j=1,2, p_{sj} is calculated from Eq. (3.4) replacing R and R_0 with R_j and R_{j0}, respectively, and the last term on the right-hand side provides the radiation coupling between the bubbles mentioned above. Solving these equations numerically, Mettin *et al.* found that, for some bubble pairs, where one bubble is a little smaller and the other bubble larger than the resonance size corresponding to the dynamical Blake threshold, the interaction force can change from attraction to repulsion as the bubbles come close to each other, although the driving frequency is much smaller than the linear resonance frequencies of the two bubbles. This result is of great interest in the context of the phenomenon of acoustic cavitation streamers since it implies the existence of a stable equilibrium distance between two strongly oscillating bubbles. However, as the authors themselves conclude, their findings are yet unable to explain the mechanism of acoustic streamer formation because of the predominant attractive situations in parameter space.

Considering the same problem, i.e., acoustic streamer formation, Doinikov [90] proposed a model that makes possible a direct calculation of the translational motion (instead of the mean forces as in [89]) of two interacting small spherical bubbles in a strong acoustic field. Using the Lagrangian formalism, he derived coupled equations of radial and translational motions of two interacting bubbles in an ideal incompressible liquid with an accuracy up to terms of third order in the inverse distance between the bubbles. The equations of radial pulsations were then modified, for the purpose of allowing for effects of liquid compressibility, using Keller-Miksis' approach, and the equations of translation were added by viscous forces in the form of the Levich drag. The resulting equations are as follows:

$$\begin{aligned}
&\left(1-\frac{\dot{R}_j}{c}\right)R_j\ddot{R}_j + \left(\frac{3}{2}-\frac{\dot{R}_j}{2c}\right)\dot{R}_j^2 - \left(1+\frac{\dot{R}_j}{c}\right)\frac{p_{sj}}{\rho_0} - \frac{R_j}{\rho_0 c}\frac{dp_{sj}}{dt} - \frac{\dot{x}_j^2}{4} \\
&= -\frac{R_{3-j}^2\ddot{R}_{3-j} + 2R_{3-j}\dot{R}_{3-j}^2}{L} - \frac{(-1)^j R_{3-j}^2(\dot{x}_j\dot{R}_{3-j} + R_{3-j}\ddot{x}_{3-j} + 5\dot{R}_{3-j}\dot{x}_{3-j})}{2L^2} - \frac{R_{3-j}^3\dot{x}_{3-j}(\dot{x}_j + 2\dot{x}_{3-j})}{2L^3},
\end{aligned} \tag{3.10}$$

$$\frac{R_j\ddot{x}_j}{3}+\dot{R}_j\dot{x}_j-\frac{(-1)^j}{L^2}\frac{d}{dt}\left(R_jR_{3-j}^2\dot{R}_{3-j}\right)-\frac{R_{3-j}^2(R_jR_{3-j}\ddot{x}_{3-j}+R_{3-j}\dot{R}_j\dot{x}_{3-j}+5R_j\dot{R}_{3-j}\dot{x}_{3-j})}{L^3}=\frac{F_{exj}}{2\pi\rho_0R_j^2}, \quad (3.11)$$

where j=1,2, p_{sj} is calculated from Eq. (3.4) replacing R and R_0 with R_j and R_{j0}, $x_j(t)$ is the instantaneous position of the center of the jth bubble, and F_{exj} denotes an external force on the jth bubble, such as viscous drag. The application of Eqs. (3.10) and (3.11) to the parameter space characteristic of acoustic streamers reveals that for most combinations of bubble radii, contrary to the predictions of [89], a mutual approach results in a dynamically equilibrium separation distance between the bubbles rather than collision and coalescence. Examples of such situations are shown in Fig. 10 for two pairs of air bubbles in water subject to a sound pressure field with a driving frequency of 20 kHz and amplitude of 1.2 bar. The lower curves correspond to bubble 1 and the upper curves to bubble 2. These results, hopefully, seem to be able to give an insight into the mechanism of acoustic streamer formation.

The results obtained in [84,85,90], when compared with those from [80,83,89], suggest that the use of time averaging in strong fields is apparently not a very good approach. In strong fields, processes occur very fast and vigorously. After time averaging, we may lose important details and make wrong inferences. This issue still remains open, though.

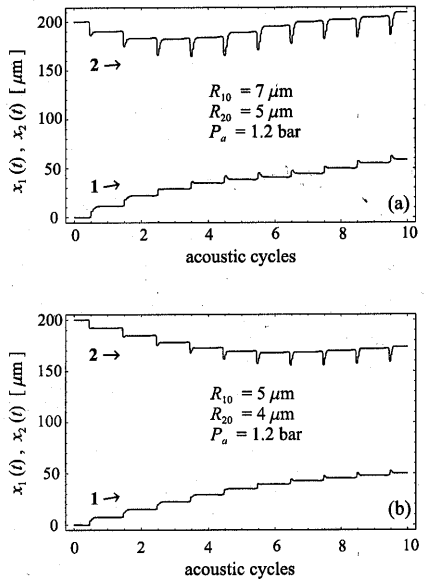

Figure 10. Examples of bubble paths obtained by means of Eqs. (3.10) and (3.11).

References

1. Jones, R.V., and Leslie, B. 1978, Proc. R. Soc. Lond. A, **360**, 347.
2. Ashkin, A. 1980, Science, **210**, 1081.
3. Trinh, E.H. 1985, Rev. Sci. Instrum., **56**, 2059.

4. Lee, C.P., Anilkumar, A.V., and Wang, T.G. 1991, Phys. Fluids A, **3**, 2497.
5. Chen, X. and Apfel, R.E. 1996, J. Acoust. Soc. Am., **99**, 713.
6. Mednikov, E.P. 1965, Acoustic Coagulation and Precipitation of Aerosols, Consultants Bureau, New York.
7. Rozenberg, L.D. (Ed.) 1973, Physical Principles of Ultrasonic Technology, Plenum, New York.
8. Hill, C.R. (Ed.) 1986, Physical Principles of Medical Ultrasonics, Ellis Horwood, New York.
9. Leighton, T.G. 1994, The Acoustic Bubble, Academic, London.
10. Brennen, C.E. 1995, Cavitation and Bubble Dynamics, Oxford U. P., London.
11. Walton, A.J., and Reynolds, G.T. 1984, Adv. Phys., **33**, 595.
12. Crum, L.A. 1994, Physics Today, **47**, 22.
13. Bjerknes, V.F.K. 1906, Fields of Force, Columbia U. P., New York.
14. König, W. 1891, Ann. Phys., **42**, 353; **42**, 549.
15. Kobelev, Yu.A., Ostrovskii, L.A., and Sutin, A.M. 1979, Pis'ma Zh. Eksp. Teor. Fiz., **30**, 423.
16. Marston, P.L., Trinh, E.H., Depew, J., and Asaki, J. 1994, Bubble Dynamics and Interface Phenomena, J.R. Blake, J.M. Boulton-Stone, and N.H. Thomas (Eds.), Kluwer Academic, Dordrecht, 343.
17. Avetisyan, A.G., Arakelyan, V.S., Bagdasaryan, O.V., and Dudoyan, A.K. 1985, Sov. Phys. Acoust., **31**, 227.
18. Akhatov, I., Parlitz, U., and Lauterborn, W. 1994, J. Acoust. Soc. Am., **96**, 3627.
19. King, L.V. 1934, Proc. R. Soc. Lond. A, **147**, 212.
20. Klein, E. 1938, J. Acoust. Soc. Am., **9**, 312.
21. Rudnick, I. 1977, J. Acoust. Soc. Am., **62**, 20.
22. Leung, E., Jacobi, N., and Wang, T. 1981, J. Acoust. Soc. Am., **70**, 1762.
23. Embleton, T.F.W. 1954, J. Acoust. Soc. Am., **26**, 40.
24. Embleton, T.F.W. 1954, J. Acoust. Soc. Am., **26**, 46.
25. Nyborg, W.L. 1967, J. Acoust. Soc. Am., **42**, 947.
26. Hasegawa, T., Ochi, M., and Matsuzawa, K. 1980, J. Acoust. Soc. Am., **67**, 770.
27. Embleton, T.F.W. 1954, J. Acoust. Soc. Am., **26**, 46.
28. Yosioka, K., and Kawasima, Y. 1955, Acustica, **5**, 167.
29. Minnaert, M. 1933, Philos. Mag., **16**, 235.
30. Boyle, R.W. 1927, Nature, **120**, 476.
31. Hopwood, F.L. 1931, Nature, **128**, 748.
32. Blake, F.G. 1949, J. Acoust. Soc. Am., **21**, 551.
33. Yosioka, K., Kawasima, Y., and Hirano, H. 1955, Acustica, **5**, 173.
34. Asaki, T.J., and Marston, P.L. 1994, J. Acoust. Soc. Am., **96**, 3096.
35. Crum, L.A. 1971, J. Acoust. Soc. Am., **50**, 157.
36. Eller, A.I. 1968, J. Acoust. Soc. Am., **43**, 170.
37. Crum, L.A. and Eller, A.I. 1970, J. Acoust. Soc. Am., **48**, 181.
38. Hasegawa, T., and Yosioka, K. 1969, J. Acoust. Soc. Am., **46**, 1139.
39. Hasegawa, T., and Yosioka, K. 1975, J. Acoust. Soc. Am., **58**, 581.
40. Hasegawa, T., Ochi, M., and Matsuzawa, K. 1981, J. Acoust. Soc. Am., **70**, 242.
41. Hasegawa, T. 1977, J. Acoust. Soc. Am., **61**, 1445.
42. Hasegawa, T., and Watanabe, Y. 1978, J. Acoust. Soc. Am., **63**, 1733.
43. Hasegawa, T. 1979, J. Acoust. Soc. Am., **65**, 32.
44. Hasegawa, T. 1979, J. Acoust. Soc. Am., **65**, 41.
45. Hasegawa, T., Ochi, M., and Matsuzawa, K. 1981, J. Acoust. Soc. Am., **69**, 937.
46. Wu, J., and Du, G. 1990, J. Acoust. Soc. Am., **87**, 997.
47. Lee, C.P., and Wang, T.G. 1988, J. Acoust. Soc. Am., **83**, 1324.
48. Lighthill, M.J. 1978, J. Sound Vib., **24**, 471.
49. Doinikov, A.A. 1994, J. Fluid Mech., **267**, 1.

50. Doinikov, A.A. 1994, Proc. R. Soc. Lond. A, **447**, 447.
51. Doinikov, A.A. 1997, J. Acoust. Soc. Am., **101**, 713.
52. Doinikov, A.A. 1997, J. Acoust. Soc. Am., **101**, 722.
53. Doinikov, A.A. 1997, J. Acoust. Soc. Am., **101**, 731.
54. Doinikov, A.A. 1998, J. Acoust. Soc. Am., **103**, 143.
55. Doinikov, A.A. 1996, J. Acoust. Soc. Am., **100**, 1231.
56. Doinikov, A.A. 1996, Wave Motion, **24**, 275.
57. Kazantsev, V.F. 1960, Sov. Phys. Dokl., **4**, 1250.
58. Crum, L.A. 1975, J. Acoust. Soc. Am., **57**, 1363.
59. Zabolotskaya, E.A. 1984, Sov. Phys. Acoust., **30**, 365.
60. Doinikov, A.A., and Zavtrak, S.T. 1995, Phys. Fluids, **7**, 1923.
61. Doinikov, A.A., and Zavtrak, S.T. 1996, J. Acoust. Soc. Am., **99**, 3849.
62. Pelekasis, N.A., and Tsamopoulos, J.A. 1993, J. Fluid Mech., **254**, 467.
63. Pelekasis, N.A., and Tsamopoulos, J.A. 1993, J. Fluid Mech., **254**, 501.
64. Nemtsov, B.E. 1983, Pis'ma Zh. Tekh. Fiz., **9**, 858 (in Russian).
65. Doinikov, A.A., and Zavtrak, S.T. 1997, J. Acoust. Soc. Am., **102**, 1424.
66. Doinikov, A.A. 1999, J. Acoust. Soc. Am., **106**, 3305.
67. Doinikov, A.A. 2002, J. Acoust. Soc. Am., **111**, 1602.
68. Alekseev, V.N. 1991, Sov. Phys. Acoust., **37**, 309.
69. Bruskin, L.G. 1991, Sov. Phys. Acoust., **37**, 428.
70. Rooney, J.A. 1970, Science, **169**, 869.
71. ter Haar, G.R., and Wyard, S.J. 1978, Ultrasound Med. Biol., **4**, 111.
72. Landau, L.D., and Lifshitz, E.M. 1959, Fluid Mechanics, Pergamon, New York.
73. Doinikov, A.A., and Zavtrak, S.T. 1996, Ultrasonics, **34**, 807.
74. Doinikov, A.A. 1996, J. Acoust. Soc. Am., **99**, 3373.
75. Alekseev, V.N. 1983, Sov. Phys. Acoust., **29**, 77.
76. Doinikov, A.A., and Zavtrak, S.T. 1991, Prikl. Mekh. Tekh. Fiz., **6**, 65.
77. Doinikov, A.A. 2001, J. Fluid Mech., **444**, 1.
78. Eller, A.I., and Crum, L.A. 1970, J. Acoust. Soc. Am., **47**, 762.
79. Mettin, R., Luther, S., Ohl, C.-D., and Lauterborn, W. 1999, Ultrason. Sonochem., **6**, 25.
80. Akhatov, I., Mettin, R., Ohl, C.D., Parlitz, U., and Lauterborn, W. 1997, Phys. Rev. E, **55**, 3747.
81. Keller, J.B., and Miksis, M. 1980, J. Acoust. Soc. Am., **68**, 628.
82. Akhatov, I., Gumerov, N., Ohl, C.D., Parlitz, U., and Lauterborn, W. 1997, Phys. Rev. Lett., **78**, 227.
83. Doinikov, A.A. 2000, Phys. Rev. E, **62**, 7516.
84. Watanabe, T., and Kukita, Y. 1993, Phys. Fluids A, **5**, 2682.
85. Doinikov, A.A. 2002, Phys. Fluids, **14**, 1420.
86. Levich, B.V. 1962, Physicochemical Hydrodynamics, Prentice-Hall, Englewood Cliffs, NJ.
87. Oguz, H., and Prosperetti, A. 1990, J. Fluid Mech., 218, 143.
88. Doinikov, A.A. 1999, Phys. Rev. E, **59**, 3016.
89. Mettin, R., Akhatov, I., Parlitz, U., Ohl, C.D., and Lauterborn, W. 1997, Phys. Rev. E, **56**, 2924.
90. Doinikov, A.A. 2001, Phys. Rev. E, **64**, № 2.